

Unifying Deep Local and Global Features for Efficient Image Search

Bingyi Cao* André Araujo* Jack Sim

Google Research, USA

{bingyi, andrearaujo, jacksim}@google.com

Abstract

A key challenge in large-scale image retrieval problems is the trade-off between scalability and accuracy. Recent research has made great strides to improve scalability with compact global image features, and accuracy with local image features. In this work, our main contribution is to unify global and local image features into a single deep model, enabling scalable retrieval with high accuracy. We refer to the new model as DELG, standing for DEep Local and Global features. We leverage lessons from recent feature learning work and propose a model that combines generalized mean pooling for global features and attentive selection for local features. The entire network can be learned end-to-end by carefully balancing the gradient flow between two heads – requiring only image-level labels. We also introduce an autoencoder-based dimensionality reduction technique for local features, which is integrated into the model, improving training efficiency and matching performance. Experiments on the Revisited Oxford and Paris datasets demonstrate that our jointly learned ResNet-50 based features outperform all previous results using deep global features (most with heavier backbones) and those that further re-rank with local features. Code and models will be released.

1. Introduction

Large-scale image retrieval is the task of searching image databases for items that are similar to a query image. This is a long-standing problem in computer vision, which saw promising results [36, 41, 42, 26] even before deep learning revolutionized the field. Central to this problem are the representations used to describe images and their similarities.

Two types of image representations are necessary for high image retrieval performance: global and local features. A global feature [26, 1, 17, 44, 45], also commonly referred to as “global descriptor” or “embedding”, summarizes the contents of an image, often leading to a compact representation; information about spatial arrangement of visual ele-

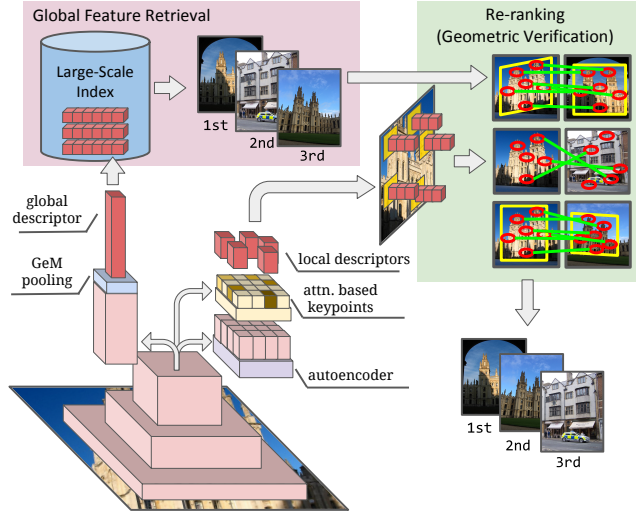


Figure 1: Our proposed DELG (DEep Local and Global features) model (bottom-left) jointly extracts deep local and global features. Global features can be used in the first stage of a retrieval system, to efficiently select the most similar images (top-left). Local features can then be employed to re-rank top results, increasing precision of the retrieved results (right). The unified model leverages hierarchical image representations induced by convolutional neural networks to learn local and global representations, combined with recent advances in global feature pooling and attentive local feature detection.

ments is lost. Local features [28, 7, 58, 37, 33], on the other hand, comprise descriptors and geometry information about specific image regions; they are especially useful to match images depicting rigid objects. Generally speaking, global features are better at recall, while local features are better at precision. Global features can learn similarity across very different poses where local features would not be able to find correspondences; contrastively, the score provided by local feature-based geometric verification usually reflects image similarity well, being more reliable than global feature distance. A common retrieval system setup is to first search by global features, then re-rank the top database images using local feature matching – to get the best of both worlds. One prominent application where such a hybrid approach gained popularity is visual localization [52, 47].

Today, most systems that rely on both these types of features need to separately extract each of them, using different

*Both authors contributed equally to this work.

models. This is undesirable since it may lead to high memory usage and increased latency, *e.g.*, if both models need to be run using specialized and limited hardware such as GPUs. Besides, in many cases similar types of computation are performed for both, resulting in redundant processing and unnecessary complexity.

Contributions. (1) Our first contribution is a unified model to represent both local and global features, using a convolutional neural network (CNN), referred to as DELG (DEep Local and Global features) – illustrated in Fig. 1. This allows for efficient inference by extracting an image’s global feature, detected keypoints and local descriptors within a single model. Our model is enabled by leveraging hierarchical image representations that arise in CNNs [59], which we couple to generalized mean pooling [44] and attentive local feature detection [37]. (2) Second, we adopt a convolutional autoencoder module that can efficiently learn low-dimensional local descriptors. This can be readily integrated into the unified model, and avoids the need of post-processing learning steps, such as PCA, that are commonly used. (3) Finally, we design a procedure that enables end-to-end training of the proposed model using only image-level supervision. This requires carefully controlling the gradient flow between the global and local network heads during backpropagation, to avoid disrupting the desired representations. Through systematic experiments, we show that our joint model achieves state-of-the-art performance on the Revisited Oxford and Paris datasets when retrieving using solely global features, or when re-ranking these results using local features.

2. Related Work

We review relevant work in local and global features, focusing mainly on approaches related to image retrieval.

Local features. Hand-crafted techniques such as SIFT [28] and SURF [7] have been widely used for retrieval problems. Early systems [31, 28, 38] worked by searching for query local descriptors against a large database of local descriptors, followed by geometrically verifying database images with sufficient number of correspondences. Bag-of-Words [51] and related methods [41, 42, 24] followed, by relying on visual words obtained via local descriptor clustering, coupled to tf-idf scoring. The key advantage of local features over global ones for retrieval is the ability to perform spatial matching, often employing RANSAC [15]. This has been widely used [41, 42, 3], as it produces reliable and interpretable scores. Recently, several deep learning-based local features have been proposed [58, 37, 32, 40, 33, 46, 14, 6]. The one most related to our work is DELF [37]; our proposed unified model incorporates DELF’s attention module, but with a much more efficient training pipeline, besides also enabling global feature extraction.

Global features. Global features excel at delivering high image retrieval performance with compact representations. Before deep learning was popular in computer vision, they were developed mainly by aggregating hand-crafted local descriptors [25, 26, 27, 54]. Today, most high-performing global features are based on deep convolutional neural networks [5, 4, 55, 1, 17, 44, 45], which are trained with ranking-based [9, 48, 19] or classification losses [57, 11]. Our work leverages recent learned lessons in global feature learning, by adopting GeM pooling [44] and ArcFace loss [11]. This leads to much improved global feature retrieval performance compared to previous techniques, which is further boosted by geometric re-ranking with local features obtained from the same model.

Joint local and global CNN features. Previous work considered convolutional neural networks for joint extraction of global and local image features. For an indoor localization application, Taira *et al.* [52] used a pre-trained VGG-based NetVLAD [1] model to extract global features for candidate pose retrieval, followed by dense local feature matching using feature maps from the same network. Simeoni *et al.*’s DSM [50] leveraged pre-trained global feature models and proposed to detect keypoints in deep activation maps using MSER [29]; the activation channels are interpreted as visual words, which can be used to propose tentative correspondences between a pair of images. Our work differs substantially from [52, 50], since they only post-process pre-trained global feature models to also produce local features, while we jointly train local and global. Sarlin *et al.* [47] distill pre-trained local SuperPoint [12] and global NetVLAD [1] features into a single model, targeting visual localization applications. In contrast, our model is trained end-to-end for image retrieval, and is not limited to mimicking separate pre-trained local and global models. To the best of our knowledge, ours is the first work to learn a non-distilled model producing both local and global image features.

Dimensionality reduction for image retrieval. PCA and whitening are widely used for dimensionality reduction of local and global features in image retrieval [4, 55, 37, 45]. As discussed in [23], whitening downweights co-occurrences of local features, which is generally beneficial for retrieval performance. Mukundan *et al.* [34] further introduce a shrinkage parameter that controls the extent of applied whitening. If supervision in the form of matching pairs or category labels is available, more sophisticated methods [30, 18] can be used. More recently, Gordo *et al.* [16] propose to replace PCA/whitening by a fully-connected layer, that is learned together with the global descriptor.

In this paper, our goal is to compose a system that can be learned end-to-end only using image-level labels, without requiring additional post-processing stages that make training more complex. Also, since we extract local features from feature maps of common CNN backbones, they tend to be

very high-dimensional and infeasible for large-scale problems. All above-mentioned approaches would either require a separate post-processing step to reduce the dimensionality of features, or supervision at the level of local patches – making them unsuitable to our needs. We thus introduce an autoencoder in our model, which can be jointly and efficiently learned with the rest of the network. It requires no extra supervision as it can be trained with a reconstruction loss.

3. DELG

3.1. Design considerations

For optimal performance, image retrieval requires semantic understanding of the types of objects that a user may be interested in, such that the system can distinguish between relevant objects versus clutter/background. Both local and global features should thus focus only on the most discriminative information within the image. However, there are substantial differences in terms of the desired behavior for these two feature modalities, posing a considerable challenge to jointly learn them.

Global features should be similar for images depicting the same object of interest, and dissimilar otherwise. This requires high-level, abstract representations that are invariant to viewpoint and photometric transformations. Local features, on the other hand, need to encode representations that are grounded to specific image regions; in particular, the keypoint detector should be equivariant with respect to viewpoint, and the keypoint descriptor needs to encode localized visual information. This is crucial to enable geometric consistency checks between query and database images, which are widely used in image retrieval systems.

Besides, our goal is to design a model that can be learned end-to-end, with local and global features, without requiring additional learning stages. This simplifies the training pipeline, allowing faster iterations and wider applicability of the model. In contrast, it is common for previous feature learning work to require several learning stages: attentive deep local feature learning [37] requires 3 learning stages (fine-tuning, attention, PCA); deep global features usually require two stages, *e.g.*, region proposal and Siamese training in [17], or Siamese training and supervised whitening in [44], or ranking loss training and PCA in [45].

3.2. Model

We design our DELG model, illustrated in Fig. 1, to fulfill the requirements outlined above. We propose to leverage hierarchical representations from CNNs [59] in order to represent the different types of features to be learned. While global features can be associated with deep layers representing high-level cues, local features are more suitable to intermediate layers that encode localized information.

Given an image, we apply a convolutional neural network backbone to obtain two feature maps: $\mathcal{S} \in \mathcal{R}^{H_S \times W_S \times C_S}$ and $\mathcal{D} \in \mathcal{R}^{H_D \times W_D \times C_D}$, representing shallower and deeper activations respectively, where H, W, C correspond to the height, width and number of channels in each case. For common convolutional networks, $H_D \leq H_S$, $W_D \leq W_S$ and $C_D \geq C_S$; deeper layers have spatially smaller maps, with a larger number of channels. Let $s_{h,w} \in \mathcal{R}^{C_S}$ and $d_{h,w} \in \mathcal{R}^{C_D}$ denote features at location h, w in these maps. For common network designs, these features are non-negative since they are obtained after the ReLU non-linearity, which is the case in our method.

In order to aggregate deep activations into a global feature, we adopt generalized mean pooling (GeM) [44], which effectively weights the contributions of each feature. Another key component of global feature learning is to whiten the aggregated representation; we integrate this into our model with a fully-connected layer $F \in \mathcal{R}^{C_F \times C_D}$, with learned bias $b_F \in \mathcal{R}^{C_F}$, similar to [17]. These two components produce a global feature $g \in \mathcal{R}^{C_F}$ that summarizes the discriminative contents of the whole image:

$$g = F \times \left(\frac{1}{H_D W_D} \sum_{h,w} d_{h,w}^p \right)^{1/p} + b_F \quad (1)$$

where p denotes the generalized mean power parameter, and the exponentiation $d_{h,w}^p$ is applied elementwise.

Regarding local features, it is crucial to select only the relevant regions for matching. This can be achieved by the addition of an attention module M [37], whose goal is to predict which among the extracted local features are discriminative for the objects of interest. This is performed as $\mathcal{A} = M(\mathcal{S})$, where M is a small convolutional network and $\mathcal{A} \in \mathcal{R}^{H_S \times W_S}$ denotes the score for each feature in \mathcal{S} .

Furthermore, since hundreds to thousands of local features are commonly used, they must be represented compactly. To do so, we propose to integrate a small convolutional autoencoder (AE) module [21], which is responsible for learning a suitable low-dimensional representation. The local descriptors are obtained as $\mathcal{L} = T(\mathcal{S})$, where $\mathcal{L} \in \mathcal{R}^{H_S \times W_S \times C_T}$, and T is the encoding part of the autoencoder, corresponding to a 1×1 convolutional layer with C_T filters. Each extracted local feature at position h, w is thus represented with a local descriptor $l_{h,w} \in \mathcal{L}$ and its corresponding keypoint detection score $a_{h,w} \in \mathcal{A}$.

Finally, the global and local descriptors are L_2 -normalized into \hat{g} and $\hat{l}_{h,w}$, respectively.

3.3. Training

We propose to train the model using only image-level labels, as illustrated in Fig. 2. In particular, note that we do not require patch-level supervision to train local features, in contrast to most recent works [14, 46, 35].

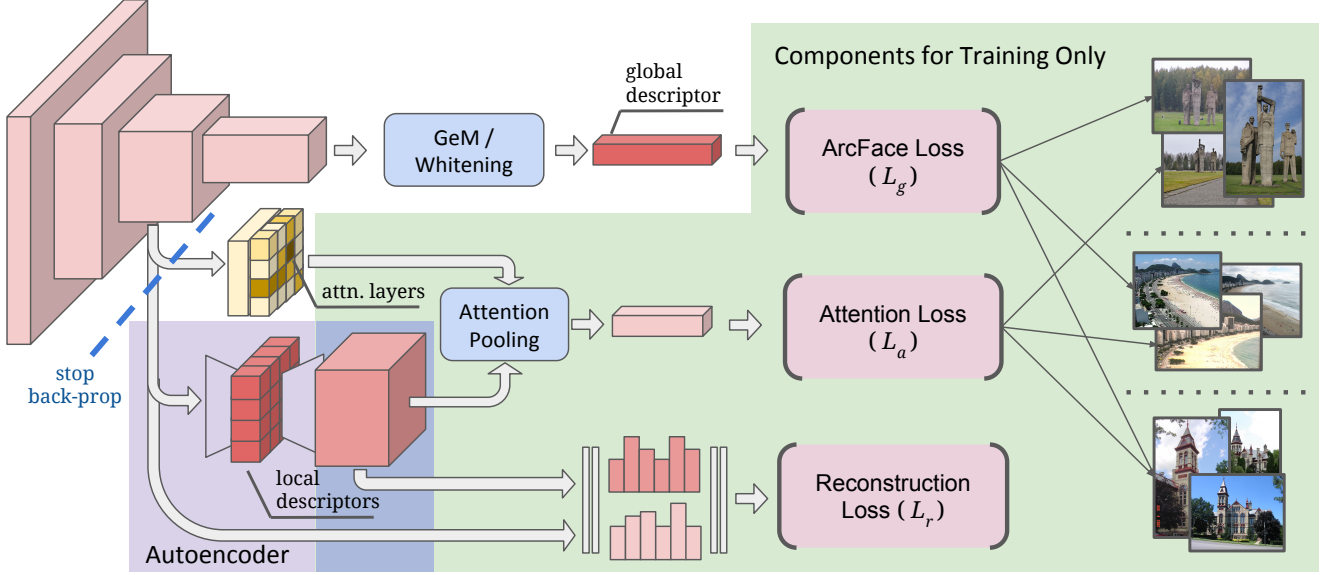


Figure 2: Illustration of our training pipeline. The components highlighted in green are used solely during training. There are two classification losses: ArcFace for global feature learning (L_g), and softmax for attention learning (L_a). In both cases, the classification objective is to distinguish different landmarks (an instance-level recognition problem). The autoencoder (purple) is further trained with a reconstruction loss (L_r). The whole model is learned end-to-end, and benefits substantially from stopping gradient propagation from L_a and L_r into the CNN backbone.

Besides the challenge to acquire the annotations, note that patch-level supervision could help selecting repeatable features, but not necessarily the discriminative ones; in contrast, our model discovers discriminative features by learning which can distinguish the different classes, given by image-level labels. In this weakly-supervised local feature setting, it is very important to control the gradient flow between the global and local feature learning, which is discussed in more detail below.

Global features. For global feature learning, we adopt a suitable loss function with L_2 -normalized classifier weights \hat{W} , followed by scaled softmax normalization and cross-entropy loss [56]; this is sometimes referred to as “cosine classifier”. Additionally, we adopt the ArcFace margin [11], which has shown excellent results for global feature learning by inducing smaller intra-class variance. Concretely, given \hat{g} , we first compute the cosine similarity against \hat{W} , adjusted by the ArcFace margin. The ArcFace-adjusted cosine similarity can be expressed as $\text{AF}(u, c)$:

$$\text{AF}(u, c) = \begin{cases} \cos(\arccos(u) + m), & \text{if } c = 1 \\ u, & \text{if } c = 0 \end{cases} \quad (2)$$

where u is the cosine similarity, m is the ArcFace margin and c is a binary value indicating if this is the ground-truth class. The cross-entropy loss, computed using softmax normalization can be expressed in this case as:

$$L_g(\hat{g}, y) = -\log \left(\frac{\exp(s \times \text{AF}(\hat{w}_k^T \hat{g}, 1))}{\sum_n \exp(s \times \text{AF}(\hat{w}_n^T \hat{g}, y_n))} \right) \quad (3)$$

where s is a learnable scalar, \hat{w}_i refers to the L_2 -normalized classifier weights for class i , y is the one-hot label vector and k is the index of the ground-truth class ($y_k = 1$).

Local features. To train the local features, we use two losses. First, a mean-squared error regression loss that measures how well the autoencoder can reconstruct \mathcal{S} . Denote $\mathcal{S}' = T'(\mathcal{S})$ as the reconstructed version of \mathcal{S} , with same dimensions, where T' is a 1×1 convolutional layer with C_S filters, followed by ReLU. The loss can be expressed as:

$$L_r(\mathcal{S}', \mathcal{S}) = \frac{1}{H_S W_S C_S} \sum_{h,w} \|s'_{h,w} - s_{h,w}\|^2 \quad (4)$$

Second, a cross-entropy classification loss that incentivizes the attention module to select discriminative local features. This is done by first pooling the reconstructed features \mathcal{S}' with attention weights $a_{h,w}$:

$$a' = \sum_{h,w} a_{h,w} s'_{h,w} \quad (5)$$

Then using a standard softmax-cross-entropy loss:

$$L_a(a', k) = -\log \left(\frac{\exp(v_k^T a' + b_k)}{\sum_n \exp(v_n^T a' + b_n)} \right) \quad (6)$$

where v_i, b_i refer to the classifier weights and biases for class i and k is the index of the ground-truth class; this tends to make the attention weights large for the discriminative features. The total loss is given by $L_g + \lambda L_r + \beta L_a$.

Controlling gradients. Naively optimizing the above-mentioned total loss experimentally leads to suboptimal results, because the reconstruction and attention loss terms significantly disturb the hierarchical feature representation which is usually obtained when training deep models. In particular, both tend to induce the shallower features \mathcal{S} to be more semantic and less localizable, which end up being sparser. Sparser features can more easily optimize L_r , and more semantic features may help optimizing L_a ; this as a result leads to underperforming local features.

We avoid this issue by stopping gradient propagation from L_r and L_a to the network backbone, *i.e.*, to \mathcal{S} . This means that the network backbone is optimized solely based on L_g , and will tend to produce the desired hierarchical feature representation. This is further discussed in the experimental section that follows.

4. Experiments

4.1. Experimental setup

Model backbone and implementation. The proposed model is implemented using Tensorflow, especially leveraging the Tensorflow-Slim model library [49]. We use ResNet-50 [20] in all experiments, and obtain the shallower feature map \mathcal{S} from the *conv4* output, and the deeper feature map \mathcal{D} from the *conv5* output. Note that the reference Tensorflow-Slim implementation introduces an extra stride at the end of *conv4*, which we also adopt – helping reduce the spatial resolution of \mathcal{S} . The number of channels in \mathcal{D} is $C_D = 2048$; GeM pooling [44] is applied with parameter $p = 3$, which is not learned. The whitening fully-connected layer, applied after pooling, produces a global feature with a dimensionality of $C_F = 2048$. The number of channels in \mathcal{S} is $C_S = 1024$; the autoencoder module learns a reduced dimensionality for this feature map with $C_T = 128$. The attention network M follows the setup from [37], with 2 convolutional layers, without stride, using kernel sizes of 1; as activation functions, the first layer uses ReLU and the second uses Softplus [13].

Training details. We learn our models using the training set of the Google Landmarks dataset (GLD) [37], which contains 1.2M images from 15k landmarks, starting from a pre-trained ImageNet model. For all learning runs, we use the following setup unless otherwise stated. The images first undergo data augmentation, by randomly cropping and slightly distorting the aspect ratio; then, they are resized to 512×512 resolution. We use a batch size of 16, and train using 21 Tesla P100 GPUs asynchronously, using 1.5M steps (corresponding to approximately 20 epochs), lasting 1.5 day. The model is optimized using stochastic gradient descent with momentum of 0.9, and a linearly decaying learning rate that reaches zero once the desired number of steps is reached. We experiment with initial learning rates $\{3 \times 10^{-4}, 10^{-3}, 3 \times 10^{-3}, 10^{-2}\}$ and report results for the

best performing one. We set the ArcFace margin $m = 0.1$, the weight for L_a to $\beta = 1$, and the weight for L_r to $\lambda = 10$.

Evaluation datasets. To evaluate our proposed model, we make use of the popular Oxford [41] and Paris [42] datasets, with revisited annotations [43], referred to as \mathcal{ROxf} and \mathcal{RPar} , respectively. There are 4993 (6322) database images in the \mathcal{ROxf} (\mathcal{RPar}) dataset, respectively, and a different query set for each, both with 70 images. Performance is measured using mean average precision (mAP). Large-scale results are further reported with the $\mathcal{R1M}$ distractor set [43], which contains 1M images. We also make use of GLD for ablation experiments.

Feature extraction and matching. For all retrieval experiments, we follow the convention from previous work [44, 17, 37] and use an image pyramid at inference time to produce multi-scale representations. For global features, we use 3 scales, $\{\frac{1}{\sqrt{2}}, 1, \sqrt{2}\}$; L_2 normalization is applied for each scale independently, then the three global features are average-pooled, followed by another L_2 normalization step. For local features, we experiment with the same 3 scales, but also with the more expensive setting from [37] using 7 image scales in total, with range from 0.25 to 2.0 (this latter setting is used unless otherwise noted). In practice, we run the local feature model for all scales, and only compute the parts that are exclusive to the global feature when needed, which saves computation. Local features are selected based on their attention scores \mathcal{A} ; a maximum of 1k local features are allowed, with a minimum attention score τ , where we set τ to the median attention score in the last iteration of training, unless otherwise noted. For local feature matching, we use RANSAC [15] with an affine model. When re-ranking global feature retrieval results with local feature-based matching, the top 100 ranked images from the first stage are considered. Our focus is on improving global and local features for image retrieval, so we do not consider techniques that post-process results such as query expansion [10, 44] or diffusion/graph traversal [22, 8]. These are expensive due to requiring additional passes over the database, but if desired could be integrated to our system and produce stronger performance.

4.2. Results

First, we present ablation experiments, to compare features produced by our joint model against their counterparts which are separately trained, and also to discuss the effect of controlling the gradient propagation. Then, we compare our models against state-of-the-art retrieval techniques.

For a fair comparison, our jointly trained features are evaluated against equivalent separately-trained models, with the same hyperparameters as much as possible. Our jointly trained global feature is compared against a separately-trained one with the exact same model, learning setup and initial weights. In the case of local features, the equivalent

DR Module	λ	Jointly trained	Stop gradients	GLD-pairs AP (%)
PCA [37]	-	\times	-	51.48
FC	-	\times	-	52.67
AE [ours]	0	\times	-	49.95
	1			51.28
	5			52.26
	10			54.21
	20			53.51
	10	\checkmark	\times	37.05
	10	\checkmark	\checkmark	53.73

Table 1: Results comparing different options for dimensionality reduction (DR) of local features, by matching image pairs from the Google Landmarks dataset (GLD).

separately-trained method corresponds to DELF [37]. DELF has three training stages: descriptor fine-tuning, attention training, PCA. For a fair comparison we re-train DELF with the exact same setup in the descriptor fine-tuning as the one used in our global feature training, then re-training attention and PCA.

Local features. As an ablation experiment, we assess the performance of our local features by matching image pairs. We select 200k pairs, each composed of a test and a train image from GLD, where in 1k pairs both images depict the same landmark, and in 199k pairs the two images depict different landmarks. We compute average precision (AP) after ranking the pairs based on the number of inliers. All variants for this experiment use τ equals to the 75th percentile attention score in the last iteration of training. Results are presented in Tab. 1.

First, we train solely the attention and dimensionality reduction modules, all methods initialized with the same weights from a separately-trained global feature model, for 500k iterations. These results are marked as not being jointly trained. It can be seen that our AE outperforms PCA and a simpler method using only a single fully-connected (FC) layer. Performance improves for the AE as λ increases from 0 to 10, decreasing with 20. Then, we jointly train the unified model; in this case, the variant that does not stop gradients to the backbone suffers a large drop in performance, while the variant that stops gradients obtains similar results as in the separately-trained case.

The reason for the poor performance of the naive jointly trained model is due to degradation of the hierarchical feature representation. This can be assessed by observing the evolution of activation sparsity in \mathcal{S} (*conv4*) and \mathcal{D} (*conv5*), as shown in Fig. 3. Generally, layers representing more abstract and high-level semantic properties (usually deeper layers) have high levels of sparsity, while shallower layers representing low-level and more localizable patterns are dense. As a reference, the ImageNet pre-trained model presents on average 45% and 82% sparsity for these two feature maps, respectively, when run over GLD images. For the naive joint training case, the activations of both layers quickly become

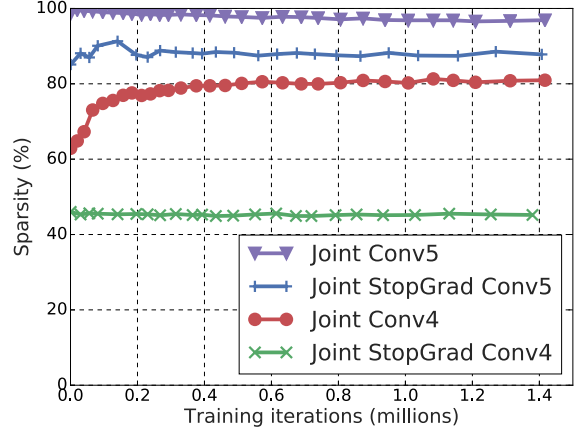


Figure 3: Evolution of activation sparsity over training iterations for \mathcal{S} (*conv4*) and \mathcal{D} (*conv5*), with the naive joint training method and our improved version that controls gradient propagation (StopGrad).

much sparser, reaching 80% and 97% at the end of training; in contrast, our proposed training scheme preserves similar sparsity as the ImageNet model: 45% and 88%. This indicates that the *conv4* features in the naive case degrade for the purposes of local feature matching; controlling the gradient effectively resolves this issue.

Global features. Tab. 2 presents experimental results comparing different global feature training methods. Naively training our unified model, without controlling gradients, underperforms when compared to the baseline separately-trained global feature, with mAP decrease of up to 5.1%. Once gradient stopping is employed, the performance can be recovered to be on par with the separately-trained version (a little better on \mathcal{ROxf} , a little worse on \mathcal{RPar}). This is expected, since the global feature in this case is optimized by itself, without influence from the local feature head.

Global+local retrieval. Tab. 2 further shows scores where the global feature-based retrieval results are re-ranked by local feature matching and spatial verification. This re-ranking step is mainly useful for the \mathcal{ROxf} dataset, and brings limited benefit in \mathcal{RPar} , which agrees with observations from previous work [53]. Our best model provides a performance boost of 5% and 7.4% on \mathcal{ROxf} Medium and Hard, respectively. The joint model which does not control gradients still shows performance gains, but smaller in both cases. Compared to the separately-trained global and local features, our best joint model obtains a similar re-ranking boost, being better in \mathcal{ROxf} -Medium and worse in the Hard case. Similarly, in terms of overall performance our joint model fares on par with the separately-trained one, being a little better in \mathcal{ROxf} , and a little worse on \mathcal{RPar} .

Comparison to state-of-the-art. Tab. 3 compares our unified model against the state-of-the-art, in three different setups: (1) local feature aggregation, followed by local feature matching and spatial verification (SP); (2) global feature

Method	Medium				Hard			
	Global	\mathcal{ROxf} + Local SP	Global	\mathcal{RPar} + Local SP	Global	\mathcal{ROxf} + Local SP	Global	\mathcal{RPar} + Local SP
Global feature training	69.3	-	82.2	-	44.4	-	64.0	-
— with separate attention & PCA [37]	-	74.1	-	82.6	-	52.4	-	63.6
— with separate attention + AE	-	74.0	-	82.6	-	51.5	-	63.9
Joint local & global training	68.8	73.0	78.9	79.3	42.4	49.5	58.3	58.4
— stop gradients [ours]	69.7	74.7	81.6	82.1	45.1	52.5	63.4	63.5

Table 2: Results (% mAP) comparing different options for global and local feature training. “Global” column indicates results using global feature similarity only; “+ Local SP” indicates that the top 100 “Global” results are re-ranked with local feature matching + spatial verification.



Figure 4: **Global feature retrieval delivers recall.** Sample DELG results on \mathcal{ROxf} -Hard (left) and \mathcal{RPar} -Hard (right), illustrating difficult, high-ranked relevant images. These database images have a low number of inliers after geometric verification (if any), which means that their similarity is mainly captured by the global feature. They present challenging cases with substantial viewpoint and lighting changes, and in some cases occlusions and blurry images – making it difficult for local feature matching to work.

similarity search; (3) same as (2), but re-ranking with local feature matching and SP.

In setup (1), we aggregate local features with or without the help of detected boxes – corresponding respectively to ASMK^* and R-ASMK^* . We take guidance from previous work [43, 53] and train codebooks of size 2^{16} , using \mathcal{ROxf} when retrieving on \mathcal{RPar} , and vice-versa. The detected boxes are obtained using the released landmark detector from [53]. Our $\text{ASMK}^* + \text{SP}$ figures outperform previously published results with other local features using this type of aggregation in all cases, except for \mathcal{RPar} -Medium. For R-ASMK^* , our results are roughly on par with [53], with small improvement in \mathcal{ROxf} -Hard and small decrease in other settings.

In setup (2), we compare global features produced by our joint model against previously published ones. Our model strongly outperforms previous work for all datasets/protocols, most noticeably in the large-scale setting, with 7.4% improvement in $\mathcal{ROxf} + \text{IM}$ -Medium and 6.1% in $\mathcal{RPar} + \text{IM}$ -Hard. Importantly, note that our model’s backbone is a ResNet-50, while the previous state-of-the-art used ResNet-101, which is much more complex (twice the



Figure 5: **Local feature re-ranking boosts precision.** Sample DELG results on \mathcal{ROxf} -Hard (top 2 queries) and \mathcal{RPar} -Hard (bottom query), illustrating performance improvements from the re-ranking stage using local features. For each query (left), two rows are presented on the right, the top one showing results based on global feature similarity and the bottom one showing results after re-ranking the top 100 images with local features. Correct results are marked in green, and incorrect ones in red.

number of floating point operations).

Finally, in setup (3) we consider the case using both global and local features. Our retrieval results provide substantial improvement over DSM [50]. The gain from spatial verification reported in their work is small, of at most 1.5% absolute across all datasets and protocols. In contrast, our re-ranking procedure significantly boosts the results from global feature retrieval, with gains of up to 8.1%, as observed in $\mathcal{ROxf} + \text{IM}$ -Hard. Our results even outperform local feature aggregation results from setup (1) in half of the cases, being better in \mathcal{RPar} and worse in \mathcal{ROxf} . We also present DELG experimental results where local feature extraction is performed with 3 scales only, the same ones used for global features. The results are very similar, providing a boost of up to 6.7%; they are at most 1.7% absolute worse than the version with 7 scales. Note that these still clearly outperform [50] and all other global feature results. Given that several recently-proposed global features [44, 17] use image pyramids with 3 scales, these results indicate that their performance can be improved substantially with negligible increase in extraction latency, and without any degradation

Method	Medium				Hard			
	\mathcal{ROxf}	$\mathcal{ROxf}+1M$	\mathcal{RPar}	$\mathcal{RPar}+1M$	\mathcal{ROxf}	$\mathcal{ROxf}+1M$	\mathcal{RPar}	$\mathcal{RPar}+1M$
Setup (1): Local feature aggregation + re-ranking								
<i>- ASMK* aggregation:</i>								
HesAff-rSIFT-ASMK*+SP [54]	60.6	46.8	61.4	42.3	36.7	26.9	35.0	16.8
HesAff-HardNet-ASMK*+SP [33]	65.6	—	65.2	—	41.1	—	38.5	—
DELf-ASMK*+SP [37, 43]	67.8	53.8	76.9	57.3	43.1	31.2	55.4	26.4
DELG-ASMK*+SP [ours]	74.6	59.3	75.6	58.2	51.9	35.9	56.7	28.1
<i>- R-ASMK* aggregation:</i>								
DELf-R-ASMK*+SP [53]	76.0	64.0	80.2	59.7	52.4	38.1	58.6	29.4
DELG-R-ASMK*+SP [ours]	75.8	63.7	79.5	59.5	53.2	39.5	58.0	29.3
Setup (2): Global features								
AlexNet-GeM [44]	43.3	24.2	58.0	29.9	17.1	9.4	29.7	8.4
VGG16-GeM [44]	61.9	42.6	69.3	45.4	33.7	19.0	44.3	19.1
ResNet101-R-MAC [17]	60.9	39.3	78.9	54.8	32.4	12.5	59.4	28.0
ResNet101-GeM [44]	64.7	45.2	77.2	52.3	38.5	19.9	56.3	24.7
ResNet101-GeM \uparrow [50]	65.3	46.1	77.3	52.6	39.6	22.2	56.6	24.8
ResNet101-GeM-AP [45]	67.5	47.5	80.1	52.5	42.8	23.2	60.5	25.1
DELG [ours]	69.7	54.9	81.6	59.7	45.1	27.8	63.4	34.1
Setup (3): Global features + Local feature re-ranking								
ResNet101-GeM \uparrow +DSM [50]	65.3	47.6	77.4	52.8	39.2	23.2	56.2	25.0
DELG (3 scales only) [ours]	73.6	59.9	82.0	60.3	50.8	34.5	62.9	34.1
DELG [ours]	74.7	60.7	82.1	60.3	52.5	35.9	63.5	34.5

Table 3: Results (% mAP) on the \mathcal{ROxf} and \mathcal{RPar} datasets (and their large-scale versions $\mathcal{ROxf}+1M$ and $\mathcal{RPar}+1M$), with both Medium and Hard evaluation protocols. We consider three different setups: (1) using local feature aggregation techniques and re-ranking; (2) using global features only; (3) using global features for initial search, then re-ranking using local features. Our results provide clear improvements against previous work in setups (2) and (3), while being on par in setup (1).

of the global feature.

Qualitative results. Qualitative DELG retrieval results are presented, showcasing the quality of the proposed model. Fig. 4 illustrates difficult retrieval cases, where the database image shows a very different viewpoint, or significant lighting changes; these images can still achieve relatively high ranks due to effective global features, which capture well the similarity even in such challenging scenarios. In these cases, local features do not produce sufficient matches.

Fig. 5 shows the effect of local feature re-ranking for selected queries, for which substantial gains are obtained. Global features tend to retrieve images that have generally similar appearance, but which sometimes do not depict the same object of interest; this can be improved substantially with local feature re-ranking, which enables stricter matching selectivity. As can be observed in these two figures, global features are crucial for high recall, while local features are key to high precision.

5. Conclusions

In this work, our main contribution is a unified model that enables joint extraction of local and global image features, referred to as DELG. The model is based on a ResNet-50 backbone, leveraging generalized mean pooling to produce global features and attention-based keypoint detection to produce local features. We further introduce an effective dimensionality reduction technique that can be integrated into

the same model, based on a convolutional autoencoder. The entire network can be trained end-to-end using image-level labels and does not require any additional post-processing steps. For best performance, we show that it is crucial to stop gradients from the attention and autoencoder branches into the network backbone, otherwise a suboptimal representation is obtained. We demonstrate the effectiveness of our approach with comprehensive experiments, achieving state-of-the-art performance in the Revisited Oxford and Paris datasets when solely using global features, or when re-ranking global feature results with local feature matching.

Appendix A. Feature Visualization

As an appendix, we provide visualizations of the features learned by the DELG model. This is useful to understand the hierarchical representation which we rely on for extraction of local and global features. We explore two types of visualizations, based on dataset examples with high activations and by optimizing input images with respect to a given layer/channel.

A.1 Feature Visualization by Dataset Examples

For this experiment, we run our DELG model over 200k images from the Google Landmarks dataset [37], and collect the images and feature positions with largest value in each channel of several activation maps. We specifically consider the activation maps at the outputs of the *conv2*, *conv3*,

conv4 and *conv5* blocks of layers in our model’s ResNet-50 architecture [20]. The feature positions with maximum activations can be mapped back to the relevant input image regions by computing the model’s receptive field parameters [2]. Note that the region may partly fall outside the image, in which case we apply zero-padding for the visualization.

Fig. 6 presents image patches that produce the highest activations for selected channels of the above-mentioned layers. The activation values are noted in each subfigure’s title and can be read by zooming in. For each selected channel of a specific layer, the 9 patches with largest activations are shown. The receptive field sizes (both horizontally and vertically) for each of these layers are: 35 (*conv2*), 99 (*conv3*), 291 (*conv4*) and 483 (*conv5*); these correspond to the sizes of image patches. One can notice that the types of patterns which maximally activate specific layers grow in complexity with network depth. This agrees with observations from previous work, where the hierarchical nature of CNN features is discussed [59, 39]. Shallower layers such as *conv2* tend to focus on edges and simple textures; *conv3* responds highly to more complex shapes, such as edges resembling palm trees (channel 15) and arches (channel 48); *conv4* focuses on object parts, such as green dome-like shapes (channel 2), or arches (channel 30); *conv5* shows strong activations for entire objects, with substantial invariances to viewpoint and lighting: entire buildings (channel 3), islands (channel 23) or towers (channel 52) are captured.

These visualizations help with intuitive understanding of our proposed method, which composes local features from a shallower layer (*conv4*) and global features from a deeper layer (*conv5*). Features from *conv5* present high degree of viewpoint invariance, being suboptimal for localized matching and more suitable to global representations. In contrast, *conv4* features seem more grounded to localizable object parts and thus can be effectively used as local feature representations.

A.2 Feature Visualization by Optimization

In this experiment, we consider the same layers and channels as above, but now adopt a visualization technique by optimizing the input image to maximally activate the desired feature. First, the input image is initialized with random noise. Given the desired layer/channel, we backpropagate gradients in order to maximally activate it. Regularizers can be useful to restrict the optimization space, otherwise the network may find ways to activate neurons that don’t occur in natural images.

We reuse the technique from Olah *et al.* [39], with default parameters, and the results are presented in Fig. 7. Again, we notice that a hierarchical representation structure forms, with more complex patterns being produced as the network goes deeper from *conv2* to *conv5*. As expected, the produced images agree very well with the patches from Fig. 6, in

terms of the types of visual contents. For example, for *conv3* channel 48, the optimized image shows arch-like edges while the dataset examples present image patches where those types of patterns occur.

Note also how deeper layers tend to specialize for the target task, by detecting image patches with parts and texture that are common to landmarks. For example, *conv4* shows detection of green dome-like shapes (channel 2) and arches (channel 30), which are common in these types of objects; *conv5*, on the other hand, shows building walls (channel 3) and rocky patterns that are common in ancient buildings or islands (channel 23).

References

- [1] R. Arandjelović, P. Gronat, A. Torii, T. Pajdla, and J. Sivic. NetVLAD: CNN Architecture for Weakly Supervised Place Recognition. In *Proc. CVPR*, 2016. 1, 2
- [2] A. Araujo, W. Norris, and J. Sim. Computing Receptive Fields of Convolutional Neural Networks. *Distill*, 2019. <https://distill.pub/2019/computing-receptive-fields>. 9
- [3] Y. Avrithis and G. Tolias. Hough Pyramid Matching: Speeded-up Geometry Re-ranking for Large Scale Image Retrieval. *IJCV*, 2014. 2
- [4] A. Babenko and V. Lempitsky. Aggregating Local Deep Features for Image Retrieval. In *Proc. ICCV*, 2015. 2
- [5] A. Babenko, A. Slesarev, A. Chigorin, and V. Lempitsky. Neural Codes for Image Retrieval. In *Proc. ECCV*, 2014. 2
- [6] A. Barroso-Laguna, E. Riba, D. Ponsa, and K. Mikolajczyk. KeyNet: Keypoint Detection by Handcrafted and Learned CNN Filters. In *Proc. ICCV*, 2019. 2
- [7] H. Bay, A. Ess, T. Tuytelaars, and L. Van Gool. Speeded-Up Robust Features (SURF). *CVIU*, 2008. 1, 2
- [8] C. Chang, G. Yu, C. Liu, and M. Volkovs. Explore-Exploit Graph Traversal for Image Retrieval. In *Proc. CVPR*, 2019. 5
- [9] S. Chopra, R. Hadsell, and Y. LeCun. Learning a Dilarity Metric Discriminatively, with Application to Face Verification. In *Proc. CVPR*, 2005. 2
- [10] O. Chum, J. Philbin, J. Sivic, M. Isard, and A. Zisserman. Total Recall: Automatic Query Expansion with a Generative Feature Model for Object Retrieval. In *Proc. ICCV*, 2007. 5
- [11] J. Deng, J. Guo, N. Xue, and S. Zafeiriou. ArcFace: Additive Angular Margin Loss for Deep Face Recognition. In *Proc. CVPR*, 2019. 2, 4
- [12] D. DeTone, T. Malisiewicz, and A. Rabinovich. SuperPoint: Self-Supervised Interest Point Detection and Description. In *Proc. CVPR Workshops*, 2018. 2
- [13] C. Dugas, Y. Bengio, C. Nadeau, and R. Garcia. Incorporating Second-Order Functional Knowledge for Better Option Pricing. In *Proc. NIPS*, 2001. 5
- [14] M. Dusmanu, I. Rocco, T. Pajdla, M. Pollefeys, J. Sivic, A. Torii, and T. Sattler. D2-Net: A Trainable CNN for Joint Detection and Description of Local Features. In *Proc. CVPR*, 2019. 2, 3

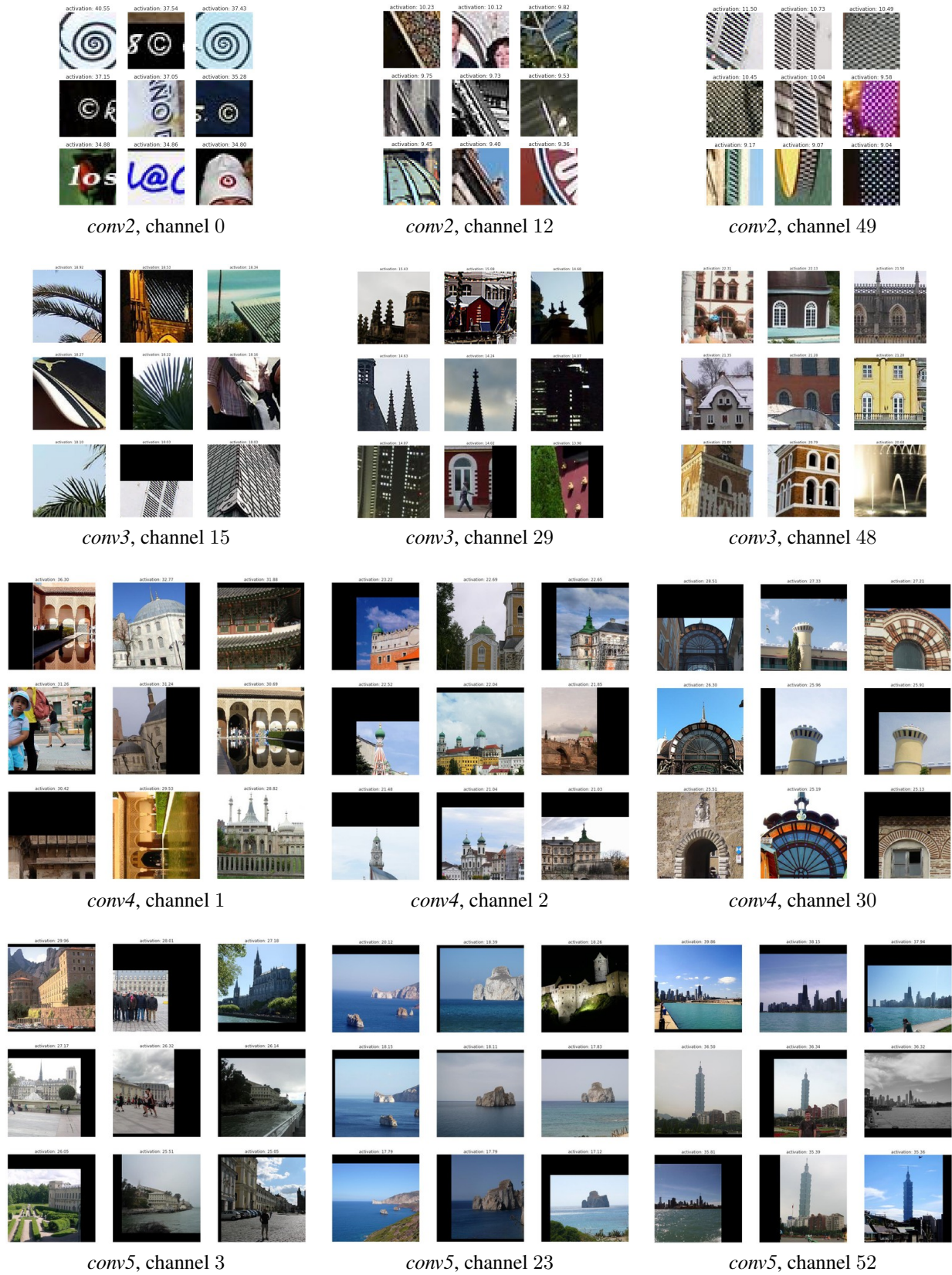


Figure 6: Visualization of patterns detected by specific feature maps / channels, by presenting image patches that produce high activations.

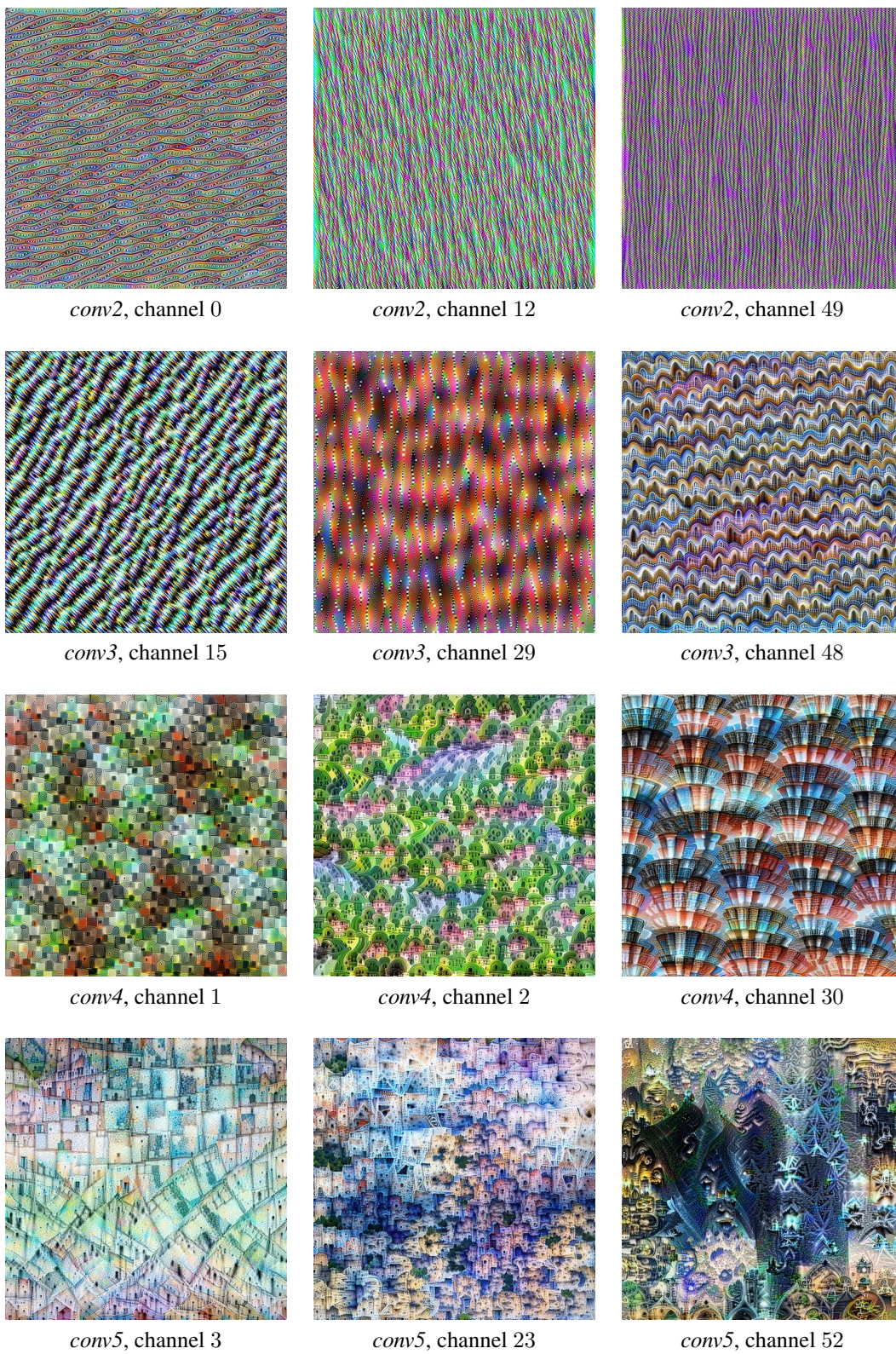


Figure 7: Visualization of patterns detected by specific feature maps / channels, by optimizing the input image to produce high activations.

- [15] M. Fischler and R. Bolles. Random Sample Consensus: A Paradigm for Model Fitting with Applications to Image Analysis and Automated Cartography. *Communications of the ACM*, 1981. 2, 5
- [16] A. Gordo, J. Almazan, J. Revaud, and D. Larlus. Deep Image Retrieval: Learning Global Representations for Image Search. In *Proc. ECCV*, 2016. 2
- [17] A. Gordo, J. Almazan, J. Revaud, and D. Larlus. End-to-end Learning of Deep Visual Representations for Image Retrieval. *IJCV*, 2017. 1, 2, 3, 5, 7, 8
- [18] A. Gordo, J. A. Rodriguez-Serrano, F. Perronin, and E. Valveny. Leveraging Category-Level Labels For Instance-Level Image Retrieval. In *Proc. CVPR*, 2012. 2
- [19] K. He, Y. Lu, and S. Sclaroff. Local Descriptors Optimized for Average Precision. In *Proc. CVPR*, 2018. 2
- [20] K. He, X. Zhang, S. Ren, and J. Sun. Deep Residual Learning for Image Recognition. In *Proc. CVPR*, 2016. 5, 9
- [21] G. Hinton. Connectionist Learning Procedures. *Artificial Intelligence*, 1989. 3
- [22] A. Iscen, G. Tolias, Y. Avrithis, T. Furon, and O. Chum. Efficient Diffusion on Region Manifolds: Recovering Small Objects with Compact CNN Representations. In *Proc. CVPR*, 2017. 5
- [23] H. Jégou and O. Chum. Negative Evidences and Co-Occurrences in Image Retrieval: The Benefit of PCA and Whitening. In *Proc. ECCV*, 2012. 2
- [24] H. Jégou, M. Douze, and C. Schmid. Hamming Embedding and Weak Geometric Consistency for Large Scale Image Search. In *Proc. ECCV*, 2008. 2
- [25] H. Jégou, M. Douze, C. Schmidt, and P. Perez. Aggregating Local Descriptors into a Compact Image Representation. In *Proc. CVPR*, 2010. 2
- [26] H. Jégou, F. Perronin, M. Douze, J. Sanchez, P. Perez, and C. Schmid. Aggregating Local Image Descriptors into Compact Codes. *IEEE Transactions on Pattern Analysis and Machine Intelligence*, 2012. 1, 2
- [27] H. Jégou and A. Zisserman. Triangulation Embedding and Democratic Aggregation for Image Search. In *Proc. CVPR*, 2014. 2
- [28] D. Lowe. Distinctive Image Features from Scale-Invariant Keypoints. *IJCV*, 2004. 1, 2
- [29] J. Matas, O. Chum, M. Urban, and T. Pajdla. Robust Wide-Baseline Stereo from Maximally Stable Extremal Regions. *Image and Vision Computing*, 2004. 2
- [30] K. Mikolajczyk and J. Matas. Improving Descriptors for Fast Tree Matching by Optimal Linear Projection. In *Proc. ICCV*, 2007. 2
- [31] K. Mikolajczyk and C. Schmid. An Affine Invariant Interest Point Detector. In *Proc. ECCV*, 2002. 2
- [32] A. Mishchuk, D. Mishkin, F. Radenovic, and J. Matas. Working Hard to Know your Neighbor's Margins: Local Descriptor Learning Loss. In *Proc. NIPS*, 2017. 2
- [33] D. Mishkin, F. Radenovic, and J. Matas. Repeatability Is Not Enough: Learning Affine Regions via Discriminability. In *Proc. ECCV*, 2018. 1, 2, 8
- [34] A. Mukundan, G. Tolias, A. Bursuc, H. Jegou, and O. Chum. Understanding and Improving Kernel Local Descriptors. *IJCV*, 2019. 2
- [35] A. Mukundan, G. Tolias, and O. Chum. Explicit Spatial Encoding for Deep Local Descriptors. In *Proc. CVPR*, 2019. 3
- [36] D. Nistér and H. Stewenius. Scalable Recognition with a Vocabulary Tree. In *Proc. CVPR*, 2006. 1
- [37] H. Noh, A. Araujo, J. Sim, T. Weyand, and B. Han. Large-Scale Image Retrieval with Attentive Deep Local Features. In *Proc. ICCV*, 2017. 1, 2, 3, 5, 6, 7, 8
- [38] S. Obdrzalek and J. Matas. Sub-linear indexing for large scale object recognition. In *Proc. BMVC*, 2005. 2
- [39] Chris Olah, Alexander Mordvintsev, and Ludwig Schubert. Feature Visualization. *Distill*, 2017. <https://distill.pub/2017/feature-visualization>. 9
- [40] Y. Ono, E. Trulls, P. Fua, and K. Moo Yi. LF-Net: Learning Local Features from Images. In *Proc. NIPS*, 2018. 2
- [41] J. Philbin, O. Chum, M. Isard, J. Sivic, and A. Zisserman. Object Retrieval with Large Vocabularies and Fast Spatial Matching. In *Proc. CVPR*, 2007. 1, 2, 5
- [42] J. Philbin, O. Chum, M. Isard, J. Sivic, and A. Zisserman. Lost in Quantization: Improving Particular Object Retrieval in Large Scale Image Databases. In *Proc. CVPR*, 2008. 1, 2, 5
- [43] F. Radenović, A. Iscen, G. Tolias, Y. Avrithis, and O. Chum. Revisiting Oxford and Paris: Large-Scale Image Retrieval Benchmarking. In *Proc. CVPR*, 2018. 5, 7, 8
- [44] F. Radenović, G. Tolias, and O. Chum. Fine-tuning CNN Image Retrieval with No Human Annotation. *IEEE Transactions on Pattern Analysis and Machine Intelligence*, 2018. 1, 2, 3, 5, 7, 8
- [45] J. Revaud, J. Almazan, R. Sampaio de Rezende, and C. Roberto de Souza. Learning with Average Precision: Training Image Retrieval with a Listwise Loss. In *Proc. ICCV*, 2019. 1, 2, 3, 8
- [46] Jerome Revaud, Cesar De Souza, Philippe Weinzaepfel, and Martin Humenberger. R2D2: Repeatable and Reliable Detector and Descriptor. In *Proc. NeurIPS*, 2019. 2, 3
- [47] P.-E. Sarlin, C. Cadena, R. Siegwart, and M. Dymczyk. From Coarse to Fine: Robust Hierarchical Localization at Large Scale. In *Proc. CVPR*, 2019. 1, 2
- [48] F. Schroff, D. Kalenichenko, and J. Philbin. FaceNet: A Unified Embedding for Face Recognition and Clustering. In *Proc. CVPR*, 2015. 2
- [49] N. Silberman and S. Guadarrama. TensorFlow-Slim Image Classification Model Library. <https://github.com/tensorflow/models/tree/master/research/slim>. 2016. 5
- [50] O. Simeoni, Y. Avrithis, and O. Chum. Local Features and Visual Words Emerge in Activations. In *Proc. CVPR*, 2019. 2, 7, 8
- [51] J. Sivic and A. Zisserman. Video Google: A Text Retrieval Approach to Object Matching in Videos. In *Proc. ICCV*, 2003. 2
- [52] H. Taira, M. Okutomi, T. Sattler, M. Cimpoi, M. Pollefeys, J. Sivic, T. Pajdla, and A. Torii. InLoc: Indoor Visual Localization with Dense Matching and View Synthesis. In *Proc. CVPR*, 2018. 1, 2

- [53] M. Teichmann, A. Araujo, M. Zhu, and J. Sim. Detect-to-Retrieve: Efficient Regional Aggregation for Image Search. In *Proc. CVPR*, 2019. 6, 7, 8
- [54] G. Tolias, Y. Avrithis, and H. Jegou. Image Search with Selective Match Kernels: Aggregation Across Single and Multiple Images. *IJCV*, 2015. 2, 8
- [55] G. Tolias, R. Sircé, and H. Jégou. Particular Object Retrieval with Integral Max-Pooling of CNN Activations. In *Proc. ICLR*, 2015. 2
- [56] F. Wang, X. Xiang, J. Cheng, and A. Yuille. NormFace: L2 Hypersphere Embedding for Face Verification. In *Proc. ACM MM*, 2017. 4
- [57] H. Wang, Y. Wang, Z. Zhou, X. Ji, Z. Li, D. Gong, J. Zhou, and W. Liu. Cosface: Large Margin Cosine Loss for Deep Face Recognition. In *Proc. CVPR*, 2018. 2
- [58] K. M. Yi, E. Trulls, V. Lepetit, and P. Fua. LIFT: Learned Invariant Feature Transform. In *Proc. ECCV*, 2016. 1, 2
- [59] M. D Zeiler and R. Fergus. Visualizing and Understanding Convolutional Networks. In *Proc. ECCV*, 2014. 2, 3, 9